

Polybenzoxazine/single-walled carbon nanotube nanocomposites stabilized through noncovalent bonding interactions



Chih-Chiao Yang^a, Yung-Chih Lin^a, Po-I. Wang^b, Der-Jang Liaw^b, Shiao-Wei Kuo^{a,*}

^aDepartment of Materials and Optoelectronic Science, Center for Nanoscience and Nanotechnology, National Sun Yat-Sen University, Kaohsiung 804, Taiwan

^bDepartment of Chemical Engineering, National Taiwan University of Science and Technology, Taipei, Taiwan

ARTICLE INFO

Article history:

Received 3 October 2013

Received in revised form

16 February 2014

Accepted 24 February 2014

Available online 5 March 2014

Keywords:

Polybenzoxazine

Carbon nanotube

Hybrid complex

ABSTRACT

In this study we prepared a new class of pyrene-functionalized benzoxazines (Py-BZ) through reactions of phenol, paraformaldehyde, and pyren-1-amine (Py-NH₂) in toluene and EtOH. We prepared Py-NH₂ through catalytic reduction of 1-nitropyrene (Py-NO₂), which we had synthesized through electrophilic aromatic substitution of pyrene, using HNO₃ as the nitration agent. ¹H and ¹³C nuclear magnetic resonance spectroscopy and Fourier transform infrared (FTIR) spectroscopy confirmed the chemical structure of this new monomer; differential scanning calorimetry (DSC) and FTIR spectroscopy revealed the curing behavior of the Py-BZ polymers. The presence of the pyrene-functionalized benzoxazine enhanced the solubility of single-walled carbon nanotubes (SWCNTs) in THF, leading to the formation of highly dispersible Py-BZ/SWCNT organic/inorganic hybrid complex materials. Fluorescence emission spectroscopy revealed significant π - π stacking interactions between the Py-BZ and the SWCNTs in these complexes. In addition, differential scanning calorimetry, thermogravimetric analysis, and dynamic mechanical analysis revealed that incorporating the SWCNTs into the Py-BZ matrix significantly enhanced the thermal stability of the polymer after thermal curing.

© 2014 Elsevier Ltd. All rights reserved.

1. Introduction

Benzoxazines are intriguing heterocyclic compounds that are attracting considerable attention for use as cyclic monomers that undergo near-zero shrinkage upon polymerization and provide polymers exhibiting tunable glass transition temperatures and high char yields [1,2]. Furthermore, polybenzoxazines (PBZs) have unique properties not found in traditional phenolic and epoxy resins, such as excellent dimensional stability, flame retardance, stable dielectric constants, and low surface free energies [3–7]. Modifications of benzoxazine resins, through the appending of alkylnyl or allyl side groups or strong hydrogen bonding functional groups, can lead to new and interesting materials for the development of useful products [8–10]. These functionalized benzoxazines can be polymerized into materials possessing three-dimensional networks exhibiting high thermal and mechanical stabilities and high resistance to solvents and moisture. Blending with other polymers [11–14], including polyurethane,

poly(ethylene oxide), and poly(*N*-vinyl-2-pyrrolidone), or organic/inorganic hybrid systems, including clay [15–17], and polyhedral oligomeric silsesquioxane (POSS) [18–26], allows further modification of the properties of benzoxazine resins.

In addition to PBZ/clay and PBZ/POSS nanocomposites [15–26], covalent surface functionalization of carbon nanotubes (CNTs) [27–29] with PBZs has also received much attention recently [30–37]. Yu et al. described the first examples of PBZ-modified multiwalled carbon nanotubes (MWCNTs) [30]. They covalently modified MWCNTs, through treatment with HNO₃ followed by toluene-2,4-diisocyanate (TDI), to introduce –OH, –CO₂H, and –N=C=O groups on their surfaces. The surface –CO₂H groups catalyzed the ring-opening reactions of benzoxazine and, thereby, decreased the curing temperature of the system. Huang et al. treated MWCNTs with H₂SO₄/HNO₃ to introduce surface –OH and –CO₂H groups [33]. These –CO₂H groups hydrogen bonded with the phenolic –OH groups after ring opening of benzoxazine, resulting in improved adhesion between PBZ and the MWCNTs. Liu et al. prepared MWCNTs modified with Diels–Alder adducts using benzoxazine functional groups [34]. Nevertheless, covalent functionalization of CNTs typically changes the orbital hybridization of some of the carbon atoms from sp² to sp³, thereby deteriorating the optical, electronic, and mechanical

* Corresponding author. Fax: +886 7 5254099.

E-mail address: kuosw@faculty.nsysu.edu.tw (S.-W. Kuo).

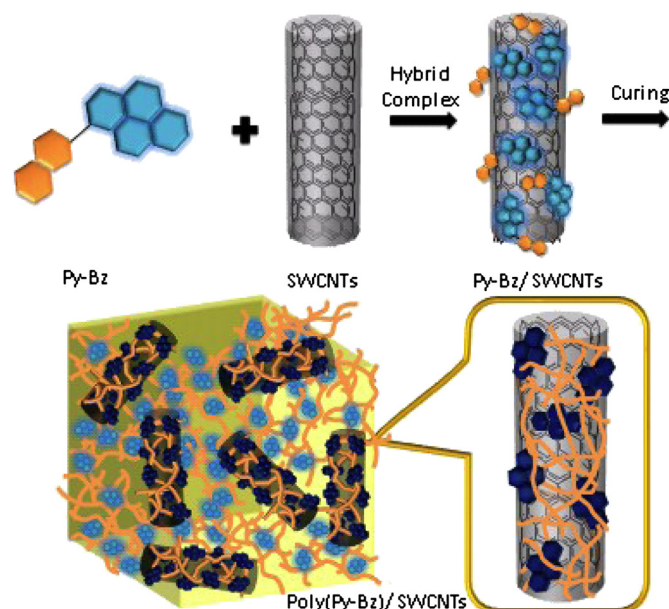
properties. Noncovalent approaches toward the modification of CNTs do not destroy the electronic conjugation, can enhance dispersibility, and can maintain the electronic and mechanical properties. Dumas et al. reported the dispersion of untreated MWCNTs in a *p*-phenylenediamine-based benzoxazine (P-pPDA) [37]. π -Stacking interactions between the CNTs and P-pPDA led to the formation of a reinforced network exhibiting enhanced thermal and mechanical properties. Most noncovalent approaches toward the modification of CNTs, however, have exploited the strong π - π interactions of pyrene with CNT surfaces [38].

Therefore, in this study we prepared a pyrene-based benzoxazine precursor that we then used to form PBZ/CNT nanocomposites, especially with single-walled carbon nanotubes (SWCNTs), stabilized through strong π - π interactions between the pyrene groups and the CNT surfaces. Electrophilic aromatic substitution of pyrene with HNO_3 as the nitration agent provided 1-nitropyrene (Py- NO_2), which we subjected to catalytic reduction to obtain pyren-1-amine (Py- NH_2). Next, we prepared a pyrene-based benzoxazine (Py-BZ) through the reaction of phenol, paraformaldehyde, and Py- NH_2 in toluene and EtOH (Scheme 1). Finally, we obtained PBZ/SWCNTs nanocomposites after mixing Py-BZ with SWCNTs and then curing. Because of the strong π - π interactions between the SWCNTs and the PBZ polymers, the systems exhibited significantly improved thermal stability, as evidenced using differential scanning calorimetry (DSC), thermogravimetric analysis (TGA), and dynamic mechanical analysis (DMA). In addition, we used fluorescence spectroscopy and transmission electron microscopy (TEM) to investigate the interactions and dispersion of SWCNTs in Py-BZ solutions Scheme 2.

2. Experimental

2.1. Materials

Paraformaldehyde (96%) and pyrene were purchased from Acros. K_2CO_3 (10 wt%) was purchased from Aldrich. Phenol (99%) was purchased from Showa. HNO_3 acid (65%) and AcOH (99.8%) were purchased from Scharlau. Hydrazine monohydrate (98%) was purchased from Alfa Aesar. SWCNTs were purchased from Centron

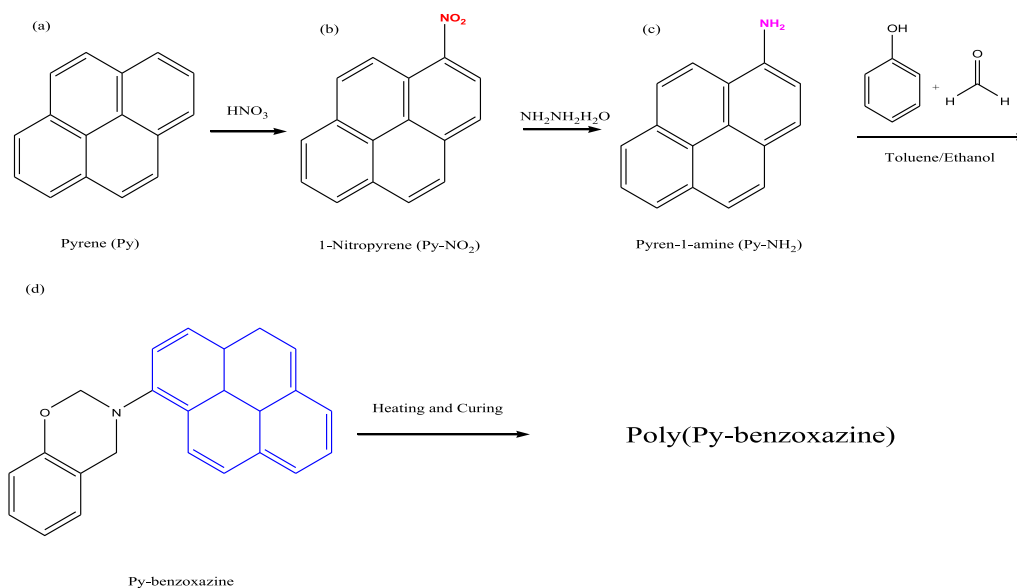


Scheme 2. Preparation of Py-BZ/SWCNT and Poly(Py-BZ)/SWCNT hybrid complexes, stabilized through π - π interactions.

Biochemistry Technology. All other chemicals were of reagent grade and used as received.

2.2. Pyren-1-amine (Py- NH_2)

A mixture of 1-nitropyrene (10 g, 4.04 mmol)—which had been prepared as yellow crystals (95%) through the nitration of pyrene with HNO_3 in AcOH and evaporation of the solvent—and palladium on carbon (0.21 g) was heated under reflux in EtOH (200 mL) for 1 h. Hydrazine hydrate (13 mL) was added and then the mixture was heated for another 1 h. After cooling, the precipitated crystals of Py- NH_2 were filtered off. The filtrate was concentrated on a vacuum rotary evaporator; cooling of the concentrate gave a second



Scheme 1. Synthesis of (b) Py- NO_2 , (c) Py- NH_2 , and (d) Py-BZ.

crop of the product. Both portions of Py-NH₂ were combined and recrystallized from cyclohexane to yield yellow crystals. The residue was purified through column chromatography (*n*-hexane/THF, 1:4) to obtain a yellow powder (70%). ¹H NMR (DMSO, ppm): 6.33 (s, 2H, CHNH₂), 7.34–8.27 (m, 9H, CCH); ¹³C NMR (DMSO, ppm): 113.05 (CHCHNH₂), 121.11–132.90 (aromatic), 144.44 (CHNH₂); IR (KBr, cm⁻¹): 3204–3463 (N–H), and elemental analysis: N: 6.3%, C: 88.5%, H: 5.2%.

2.3. 3-(Pyren-1-yl)-3,4-dihydro-2H-benzoxazine (Py-BZ)

A solution of phenol (3.46 g, 3.68 mmol) in toluene and EtOH (4:1, 10 mL) was added to an ice-cooled solution of Py-NH₂ (8.00 g, 3.68 mmol) and paraformaldehyde (2.20 g, 7.36 mmol) in toluene and EtOH (4:1, 60 mL) in a 100-mL three-necked flask and then the mixture was heated under reflux at 100 °C for 8 h. After cooling to room temperature, the filtrate was concentrated on a vacuum rotary evaporator; cooling of the concentrate gave a second crop of the product. Both portions of Py-BZ were combined and the residue was purified through column chromatography (*n*-hexane/THF, 1:4) to obtain a pale-yellow powder (50%). ¹H NMR (DMSO, ppm): 4.80 (s, 2H, CHCH₂N), 5.53 (s, 2H, OCH₂N), 6.87 (1H, CHCHCCH₂N), 7.06 (1H, CHCHCOCH₂N), 7.14 (1H, CHCCH₂N); ¹³C NMR (DMSO, ppm): 51.93 (CHCH₂N), 81.67 (OCH₂N), 116.39–131.13 (aromatic), 144.02 (COCH₂N), 153.80 (NCCC); IR (KBr, cm⁻¹): 941 (oxazine), 1232 (Ar–O–C), and elemental analysis: N: 3.7%, C: 84.6%, H: 5.7%.

2.4. Py-BZ/SWCNT nanocomposites

Py-BZ and SWCNTs were both dissolved in THF after ultrasonication for 10 min; their solutions were left to dry in air prior to curing. Desired amounts of the SWCNTs and Py-BZ monomer were stirred in THF for 12 h at room temperature and then dried in a vacuum oven. All of the nanocomposites were polymerized in a stepwise manner: at 110 °C for 4 h, 160 °C for 3 h, 180 °C for 2 h, 200 °C for 2 h, 220 °C for 1 h, and 240 °C for 0.5 h. Each cured sample had a dark-red color.

2.5. Characterization

¹H and ¹³C nuclear magnetic resonance (NMR) spectra were recorded using an INOVA 500 instrument, with DMSO as the solvent and TMS as the external standard. Chemical shifts are reported in parts per million (ppm). Fourier transform infrared (FTIR) spectra of the polymer blend films were recorded using a Bruker Tensor 27 FTIR spectrophotometer and the conventional KBr disk method; 32 scans were collected at a spectral resolution of 1 cm⁻¹. The films used in this study were sufficiently thin to obey the Beer–Lambert law. FTIR spectra recorded at elevated temperatures were obtained from a cell mounted inside the temperature-controlled compartment of the spectrometer. Dynamic curing kinetics were determined using a TA Q-20 differential scanning calorimeter operated under a N₂ atmosphere. The sample (ca. 7 mg) was placed in a sealed aluminum sample pan. Dynamic curing scans were recorded from 30 to 350 °C at a heating rate of 10 °C/min. Glass transition temperatures were determined after scanning at a rate of 20 °C/min over a temperature range from 30 to 250 °C. The measurement was made after placing a sample (5–10 mg) on a DSC sample cell and quickly cooling to –100 °C from the melt of the first scan. The glass transition temperature was taken as the midpoint of the heat capacity transition between the upper and lower points of deviation from the extrapolated liquid and glass lines. The thermal stability of the samples was measured using a TA Q-50 thermogravimetric analyzer operated under a N₂ atmosphere. The cured sample (ca. 7 mg) was placed in a Pt cell and heated at a rate of 20 °C/min from

30 to 800 °C under a N₂ flow rate of 60 mL/min. The preparation of the samples for DMA, we placed the sample powder sandwiched in the middle of single cantilever bending, measured at room temperature to 250 °C. DMA was performed using a Perkin–Elmer Instruments DMA 8000 apparatus operated in tension mode over a temperature range from 30 to 250 °C. Analyses of the loss tangent (tan δ) were recorded automatically by the system. The heating rate and frequency were fixed at 2 °C/min and 1 Hz, respectively. Photoluminescence (PL) excitation and emission spectra were collected at room temperature using a monochromatized Xe light source. TEM images were recorded using a JEOL-2100 transmission electron microscope operated at an accelerating voltage of 200 kV.

3. Results and discussion

3.1. Synthesis of Py-BZ

Fig. 1 presents the ¹H NMR spectra of Py-NH₂ and Py-BZ. The spectrum of Py-NH₂ [Fig. 1(a)] features a signal at 6.33 ppm corresponding to amino protons; the aromatic protons of the pyrene groups appear as a multiplet at 7.35–8.25 ppm. The spectrum of Py-BZ [Fig. 1(b)] features two peaks at 4.80 and 5.52 ppm corresponding to the protons of the CH₂ bridge of the oxazine unit [8]; the amino protons of Py-NH₂ are absent, but the signals for the pyrene moiety are present, confirming the successful synthesis of Py-BZ. Fig. 2 presents the ¹³C NMR spectra of Py-NH₂ and Py-BZ. In Fig. 2(a), the signals of the pyrenyl aromatic ring of Py-NH₂ appear in the range from 113.1 to 144.4 ppm. Two peaks appear at 51.8 and 81.6 ppm in the spectrum of Py-BZ in Fig. 2(b), representing the resonances of the carbon nuclei of the oxazine ring; the signals of the pyrenyl aromatic ring were evident, confirming the successful synthesis of Py-BZ. Fig. 3 presents room-temperature FTIR spectra of Py-NH₂, Py-BZ, and, after thermal curing, poly(Py-BZ). The spectrum of Py-NH₂ reveals [Fig. 3(a)] a sharp signal for the amino group at 3200–3460 cm⁻¹ and absorption bands of the pyrene unit at 831, 1599, 1619, and 3033 cm⁻¹. In the spectrum of Py-BZ [Fig. 3(b)], the signal for the amino group is absent, but signals are evident for the C–C stretching vibrations of the 1,2,4-substituted benzene ring at 1493 and 941 cm⁻¹ for the oxazine ring and for the asymmetric C–O–C stretching at 1229 cm⁻¹. Together, these spectroscopic data confirmed the successful synthesis of Py-BZ. In addition, Fig. 3(c) presents FTIR spectra recorded after each curing cycle of pure Py-BZ. The characteristic absorption

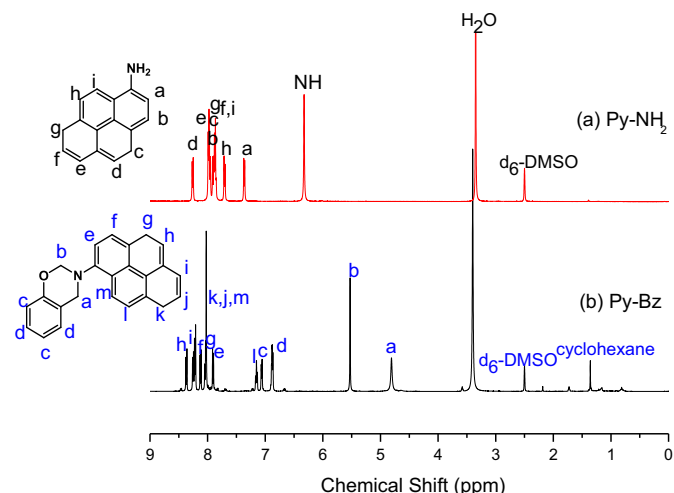


Fig. 1. ¹H NMR spectra of (a) Py-NH₂ and (b) Py-BZ.

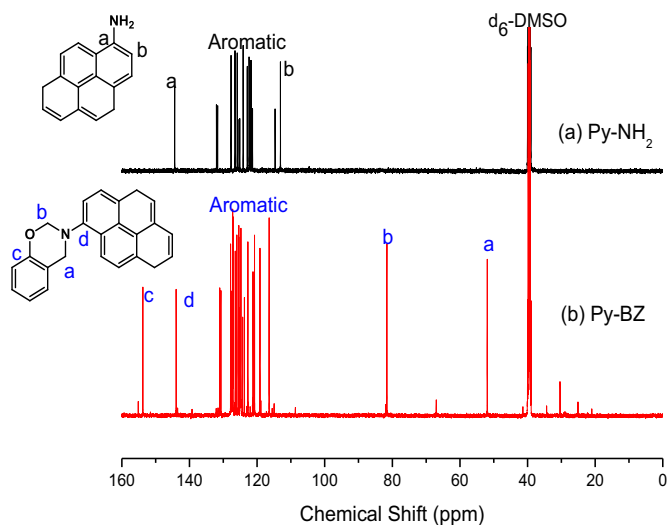


Fig. 2. ^{13}C NMR spectra of (a) Py-NH₂ and (b) Py-BZ.

bands of the trisubstituted aromatic ring of Py-BZ (1493 and 941 cm^{-1}) disappeared after thermal curing. The broad absorption bands at 2500–3500 cm^{-1} in Fig. 3(c) represent three different kinds of hydrogen bonding interactions: $[\text{O}^-\cdots\text{H}-\text{N}^+]$ intramolecular hydrogen bonding near 2700 cm^{-1} , $[\text{O}-\text{H}\cdots\text{N}]$ intramolecular hydrogen bonding near 3230 cm^{-1} , and $[\text{O}-\text{H}\cdots\text{O}]$ intermolecular hydrogen bonding near 3400 cm^{-1} ; the identities of these signals have been discussed previously [39].

3.2. Thermal polymerization Py-BZ

We used DSC to investigate the curing behavior of pure Py-BZ [Fig. 4]. The DSC trace of the uncured Py-BZ features a sharp melting point at 110 °C, revealing the high purity of the Py-BZ monomer, as well as an exotherm with a maximum at 286.0 °C and a reaction heat of 209.3 J/g. After thermal curing of pure Py-BZ at 160 °C, the first melting peak was absent from the DSC curve. The intensity of the exotherm decreased upon increasing the curing temperature, almost disappearing after curing at temperatures between 160 and 200 °C. We observed a glass transition for the

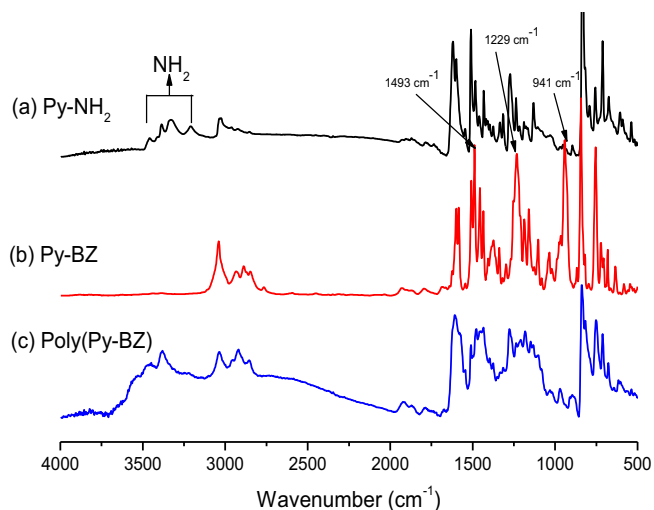


Fig. 3. FTIR spectra of (a) Py-NH₂, (b) Py-BZ, and (c) poly(Py-BZ), recorded at room temperature.

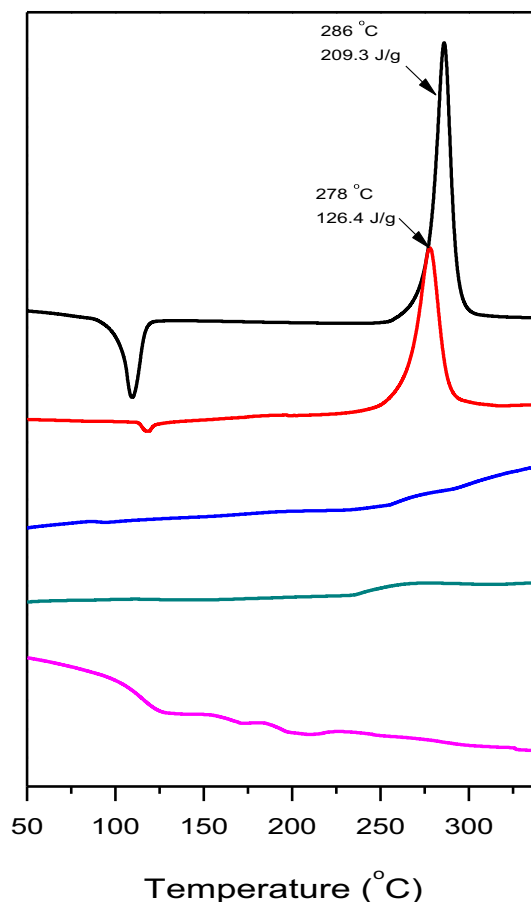


Fig. 4. DSC thermograms of the Py-BZ monomer recorded after each heating stage.

poly(Py-BZ) at 116 °C after thermal curing at 240 °C. To ascertain the types of reactions occurring during each exotherm in the DSC traces, we used FTIR spectroscopy to characterize the curing processes of the pure Py-BZ systems at various temperatures. Fig. 5 presents IR spectra recorded after each curing cycle of pure Py-BZ. The characteristic absorption bands of the trisubstituted aromatic ring of Py-BZ at 941 cm^{-1} disappeared after thermal curing at 180 °C.

3.3. Thermal properties of Py-BZ/SWCNT nanocomposites

Fig. 6 displays photographs of THF solutions of pure Py-BZ, pure SWCNTs, and Py-BZ in the presence of the pure SWCNTs. Pure Py-BZ formed a clear solution, whereas the pure SWCNTs precipitated completely; the addition of the Py-BZ into the suspension of the SWCNTs resulted in a clear brown solution (placed seven days), indicating that soluble complexes were formed as a result of non-covalent interactions (presumably primarily π - π stacking). We used TEM to further investigate the morphologies of the dispersions of the Py-BZ/SWCNT hybrid complexes after ultrasonication. On the basis of spontaneous formation of Py-BZ hybrid complexes through π - π stacking with the SWCNTs, Fig. 6(d) displays a uniform dispersion of the SWCNTs within the Py-BZ matrix. Fig. 7 displays fluorescence spectra of Py-BZ and the Py-BZ/SWCNT complexes in solution after excitation at 343 nm. The spectrum of Py-BZ features strong signals for the fluorescence of the pyrene units at 406 and 429 nm; the spectra of the Py-BZ/SWCNT complexes exhibited very weak excimer fluorescence and quenched monomer fluorescence [35]. These findings suggest that most of the pyrene moieties of Py-

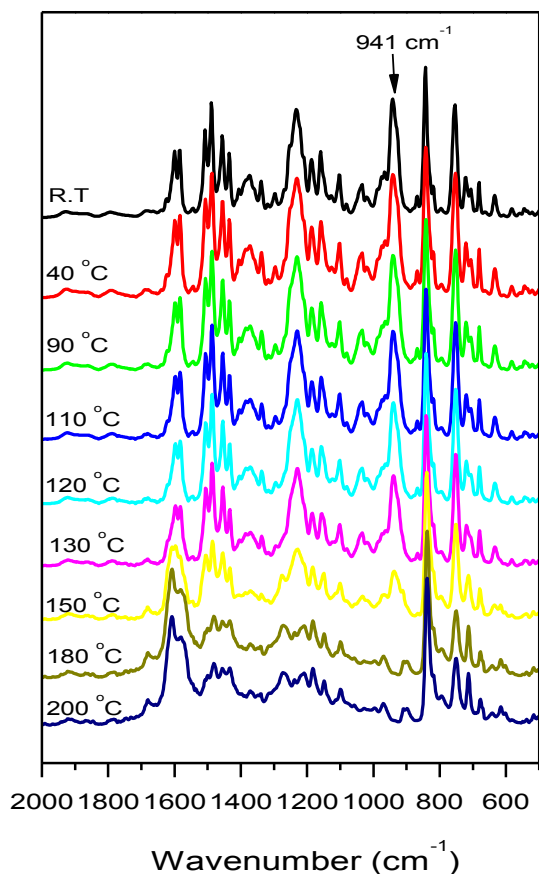


Fig. 5. FTIR spectra of the Py-BZ monomer recorded after each heating stage.

BZ interacted with the SWCNTs through π – π stacking, with only a few of them available for excimer formation as a result of steric hindrance; therefore, our proposed model consists of coexisting Py-BZ (Py/Py excimer) and Py-BZ/SWCNT nano hybrids.

Fig. 8 presents the DSC profiles of Py-BZ and the Py-BZ/SWCNT nano hybrids. Both the onset and maximum exothermic temperatures decreased significantly upon increasing the SWCNT content, implying increasingly faster thermal curing of the benzoxazine monomers. Some studies confirmed that CNTs could act as a catalyst for polymer resins and initiate early state curing [8,35,36]. Thus, we attribute the decrease in the curing temperatures to the catalytic effect of the SWCNTs on the benzoxazine ring-opening reaction, thereby accelerating the curing process at lower temperatures. For example, the exotherm peak for Py-BZ blended with 3 wt% SWCNT

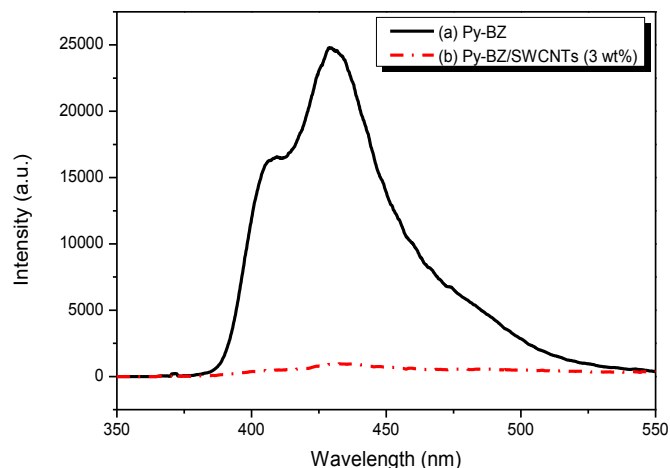


Fig. 7. PL spectra of (a) Py-BZ and (b) the Py-BZ/SWCNT (3 wt%) hybrid complex.

appeared at 238 °C, approximately 48 °C lower than that of pure Py-BZ. The total exotherm for this blend was 100.3 J/g, lower than that of pure Py-BZ, as would be expected. The reduction of enthalpy was also due to the catalytic effect of the CNTs added and the addition of CNTs physically hindered the mobility of the polymer chains and the crosslinking reaction of polybenzoxazine [36].

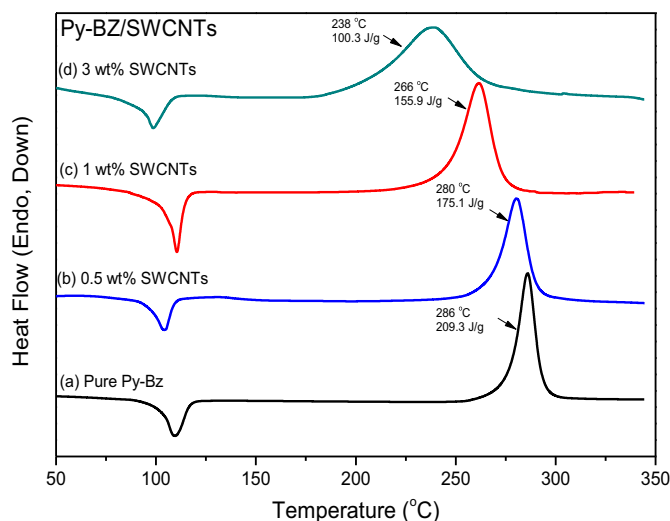


Fig. 8. DSC analyses of the curing behavior of Py-BZ mixtures at various SWCNT contents.

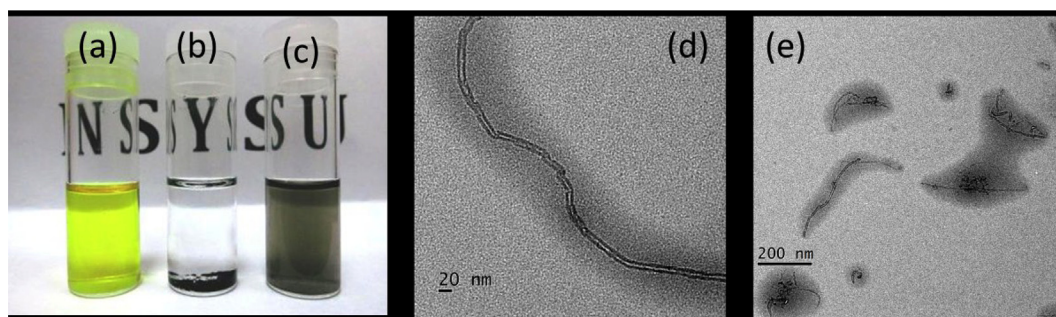


Fig. 6. (Left) Photograph of (a) pure Py-BZ, (b) the pristine SWCNTs, and (c) Py-BZ/SWCNT hybrid complexes in THF, (d) TEM image of sample (c), and (e) thermal curing of sample (d).

We used DSC to examine the glass transition behavior of poly(Py-BZ) and its blends with various amounts of SWCNTs (Fig. 9). For the pure poly(Py-BZ), the glass transition temperature (T_g) was 116 °C. In its blends with 0.5, 1, 3, and 5 wt% of SWCNTs, the values of T_g were 139, 147, 149, and 137 °C, respectively. Thus, the value of T_g of poly(Py-BZ) increased by up to 33 °C upon increasing the content of SWCNTs up to 3 wt%. However, it decreases the T_g behavior at 5 wt% to 137 °C, but still higher than pure poly(Py-BZ), presumably of two opposing effects of the CNT on the matrices. One, the nano-reinforcement effect of CNT on the polybenzoxazine matrix, tended to increase the thermal property of the material; the other, the inclusion of CNT in the system, decreased the cross-linking density of the nanocomposites as shown in Fig. 8. In a network structure, the value of T_g relates directly to the cross-linking density. We also used DMA to examine the behavior of the glass transitions of the pure poly(Py-BZ) and its blend with 3 wt% SWCNT; Fig. 10 reveals that the values of T_g were 130 and 156 °C, respectively, as determined from the maxima of the $\tan \delta$ plots; these values are slightly higher than those from the DSC analyses, as would be expected. In Fig. 8, we found that the change in the heat of reaction decreased continuously upon increasing the SWCNT content, suggesting a decrease in the degree of curing and an increase in viscosity. This decrease in the heat of reaction was due to the catalytic effect of the SWCNTs. In addition, the CNTs also imparted a steric hindrance effect on the crosslinking reaction of PBZ, thereby resulting in higher values of T_g . At relatively high SWCNT content of 5 wt%, the glass transition temperature decreased as a result of a relatively low crosslinking density and possible aggregation of SWCNTs.

Fig. 11 displays TGA thermograms of the pure poly(Py-BZ) and of the poly(Py-BZ)/SWCNTs nanohybrids under N_2 . To compare their thermal stabilities, we used the 10 wt% weight loss temperature as a standard; in the presence of 0, 0.5, 1, 3, and 5 wt% of SWCNTs, the decomposition temperatures (T_d) were 293, 338, 352, 393, and 426 °C, respectively. Thus, the values of T_d of the poly(Py-BZ)/SWCNTs nanocomposites gradually increased upon increasing the SWCNT content to 5 wt% (increasing by ca. 133 °C). The variation in thermal stability, as measured in terms of the decomposition temperature, may be construed as an effect of creating nanocomposites. In a nanocomposite material, thermal motion of the tether units is restricted, thereby minimizing the number of organic

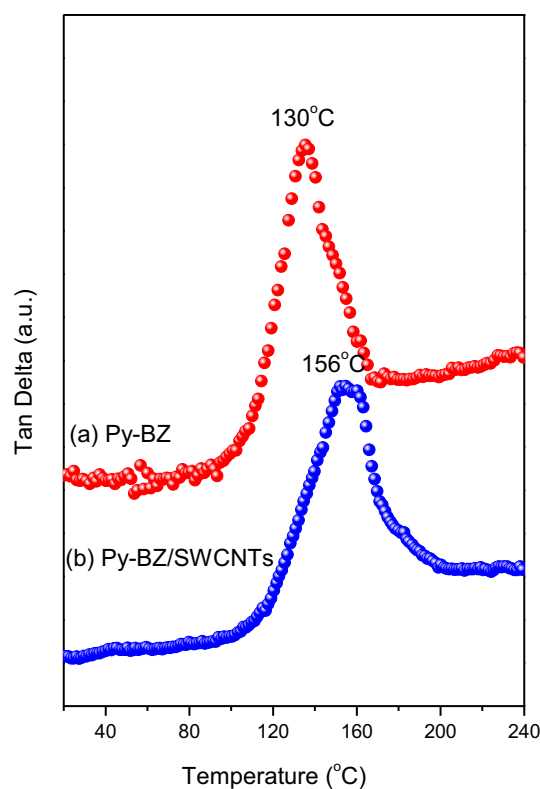


Fig. 10. DMA analyses of (a) pure Py-BZ and (b) the Py-BZ/SWCNT (3 wt%) hybrid, after curing.

decomposition pathways accessible to the tether. The char yield, another indicator of thermal stability, also increased upon increasing the content of SWCNTs to 5 wt% (relative to Py-BZ monomer) in these hybrid materials. This is because the introduction of CNT is sufficient to block the premature evaporation of the decomposed molecular fragments and for these hybrids, increasing the SWCNTs content to a certain extent did improve the composite's thermal properties [40]. Indeed, the thermal stability of the PBZs improved through the formation of network structures after incorporating inorganic CNTs.

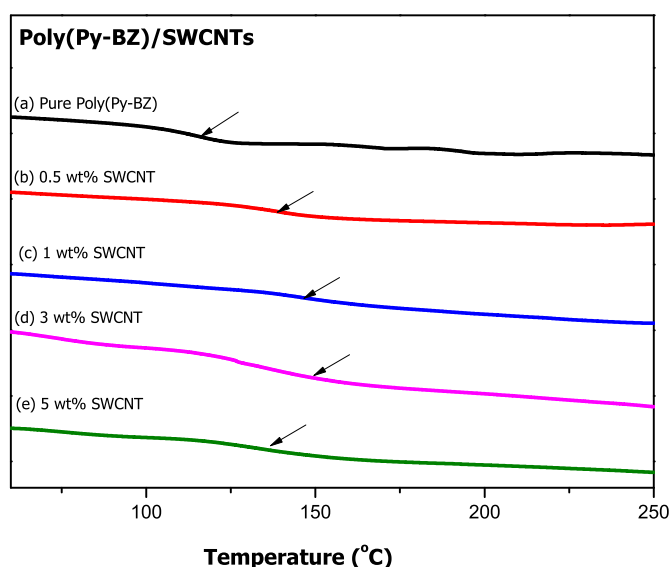


Fig. 9. DSC analyses of Py-BZ mixtures at various SWCNT contents, after curing.

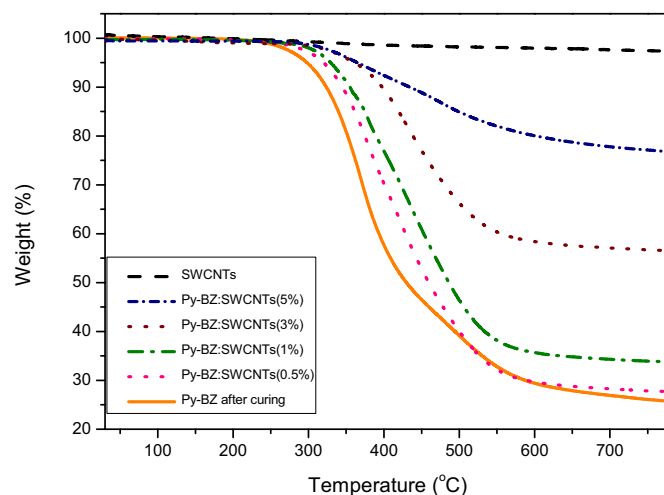


Fig. 11. TGA analyses of Py-BZ and its mixtures containing various SWCNTs contents, after curing.

4. Conclusions

We have synthesized a novel pyrene-functionalized benzoxazine that enhances the solubility of SWCNTs in THF, leading to the formation of highly dispersible Py-BZ/SWCNT organic/inorganic hybrid complex materials. The incorporation of SWCNTs into the Py-BZ matrix appeared to catalyze the polymerization, as evidenced by decreased thermal curing temperatures. Because of the crosslinked structures and the presence of the inorganic SWCNTs, the values of T_g and T_d of the poly(Py-BZ)/SWCNT hybrid complexes were higher than those of the pure poly(Py-BZ), a result of strong π – π interactions between Py-BZ and the SWCNTs.

Acknowledgments

This study was supported financially by the National Science Council, Taiwan, Republic of China, under contracts NSC 100-2221-E-110-029-MY3 and NSC 100-2628-E-110-001. We thank Mr. Hsien-Tsan Lin of the Regional Instruments Center at National Sun Yat-Sen University for help with the TEM experiments.

References

- [1] Takeichi T, Kawauchi T, Agag T. *Polym J* 2008;40:1121.
- [2] Ishida H, Allen DJ. *J Polym Sci Part B Polym Phys* 1996;34:1019.
- [3] Yagci Y, Kiskan B, Ghosh NN. *J Polym Sci Part A Polym Chem* 2009;47:5565.
- [4] Wang CF, Su YC, Kuo SW, Huang CF, Sheen YC, Chang FC. *Angew Chem Int Ed* 2006;45:2248.
- [5] Kuo SW, Wu YC, Wang CF, Jeong KU. *J Phys Chem C* 2009;113:20666.
- [6] Wang CF, Chiou SF, Ko FH, Chen JK, Chou CT, Huang CF, et al. *Langmuir* 2007;23:5868.
- [7] Wang CF, Chang FC, Kuo SW. *Hand book of polybenzoxazine*, vol. 33; 2011. p. 579.
- [8] Ishida H. *Handbook of polybenzoxazine*, vol. 1; 2011. p. 1.
- [9] Li X, Gu Y. *Polym Chem* 2011;2:2778.
- [10] Hu WH, Huang KW, Kuo SW. *Polym Chem* 2012;3:1546.
- [11] Ishida H, Lee YH. *Polymer* 2001;42:6971.
- [12] Takeichi T, Agag T, Zeidam R. *J Polym Sci Part A Polym Chem* 2001;39:2633.
- [13] Takeichi T, Guo Y. *Polym J* 2001;33:437.
- [14] Su YC, Kuo SW, Xu HY, Chang FC. *Polymer* 2003;44:2187.
- [15] Fu HK, Huang CF, Kuo SW, Lin HC, Yei DR, Chang FC. *Macromol Rapid Commun* 2008;29:1216.
- [16] Cui HW, Kuo SW. *J Polym Res* 2013;20:114.
- [17] Agag T, Takeichi T. *Polymer* 2000;41:7083.
- [18] Zhang J, Xu R, Yu D. *Eur Polym J* 2007;43:743.
- [19] Chen Q, Xu R, Zhang J, Yu D. *Macromol Rapid Commun* 2005;26:1878.
- [20] Liu Y, Zheng S. *J Polym Sci Part A Polym Chem* 2006;44:1168.
- [21] Huang JM, Kuo SW, Huang HJ, Wang YX, Chen YT. *J Appl Polym Sci* 2009;111:628.
- [22] Wu YC, Kuo SW. *Polymer* 2010;51:3948.
- [23] Huang KW, Kuo SW. *Macromol Chem Phys* 2010;211:2301.
- [24] Huang KW, Kuo SW. *Polym Comp* 2011;32:1086.
- [25] Kuo SW, Chang FC. *Prog Polym Sci* 2011;36:1649.
- [26] Hu WH, Huang KW, Chiou CW, Kuo SW. *Macromolecules* 2012;45:9020.
- [27] Frey CH. *Polymer* 2013;54:5443.
- [28] Petrov PD, Georgiev GL, Muller AHE. *Polymer* 2012;53:5502.
- [29] Liang YY, Xu JZ, Liu XY, Zhong GJ, Li ZM. *Polymer* 2013;54:6479.
- [30] Chen Q, Xu R, Yu D. *Polymer* 2006;47:7711.
- [31] Yang L, Zhang C, Pilla S, Gong S. *Compos Part A* 2008;A39:1653.
- [32] Liu Y, Wang B, Jing X. *Polym Comp* 2011;32:1352.
- [33] Huang JM, Tsai MF, Yang SJ, Chiu WM. *J Appl Polym Sci* 2011;122:1898.
- [34] Chang CM, Liu YL. *ACS Appl Mater Interfaces* 2011;3:2204.
- [35] Chapartegui M, Barcena J, Irastorza X, Elizetxea C, Fernandez M, Santamaria A. *Comp Sci Tech* 2012;72:489.
- [36] Kaleemullah M, Khan SU, Kim JK. *Comp Sci Tech* 2012;72:1968.
- [37] Dumas L, Bonnaud L, Olivier M, Dubois P. *Chem Commun* 2013;49:9543.
- [38] Murakami H, Nomura T, Nakashima N. *Chem Phys Lett* 2003;378:481.
- [39] Kim HD, Ishida H. *J Phys Chem A* 2002;106:3271.
- [40] Meng F, Ishida H, Liu X. *RSC Adv* 2014;4:9741.